



HAL
open science

Numerical Simulations for the Wake Prediction of a Marine Propeller in Straight-Ahead Flow and Oblique Flow

Emmanuel Guilmineau, Ganbo Deng, Alban Leroyer, Patrick Queutey, Michel Visonneau, Jeroen Wackers

► **To cite this version:**

Emmanuel Guilmineau, Ganbo Deng, Alban Leroyer, Patrick Queutey, Michel Visonneau, et al.. Numerical Simulations for the Wake Prediction of a Marine Propeller in Straight-Ahead Flow and Oblique Flow. *Journal of Fluids Engineering*, 2018, 140 (2), 10.1115/1.4037984 . hal-02391218

HAL Id: hal-02391218

<https://hal.science/hal-02391218>

Submitted on 28 Nov 2023

HAL is a multi-disciplinary open access archive for the deposit and dissemination of scientific research documents, whether they are published or not. The documents may come from teaching and research institutions in France or abroad, or from public or private research centers.

L'archive ouverte pluridisciplinaire **HAL**, est destinée au dépôt et à la diffusion de documents scientifiques de niveau recherche, publiés ou non, émanant des établissements d'enseignement et de recherche français ou étrangers, des laboratoires publics ou privés.

Numerical Simulations for the Wake Prediction of a Marine Propeller in Straight-Ahead Flow and Oblique Flow

E. Guilmineau, G. B. Deng, A. Leroyer, P. Queutey, M. Visonneau, J. Wackers

LHEEA, CNRS 6598, Ecole Centrale de Nantes 1 rue de la Noë BP 92101, Nantes Cedex 3 44321, France

This paper presents the capability of a numerical code, ISIS-CFD, based on the solution of the Navier–Stokes equations, for the investigation on the hydrodynamic characteristics of a marine propeller in open water. Two propellers are investigated: the Istituto Nazionale per Studi ed Esperienze di Architettura Navale (INSEAN) E779A model in straight-ahead flow and the Potsdam Propeller Test Case (PPTC) model in oblique flow. The objectives of this study are to establish capabilities of various turbulent closures to predict the wake propeller and to predict the instability processes in the wake if it exists. Two Reynolds-averaged Navier–Stokes (RANS) models are used: the k - ω shear stress transport (SST) of Menter and an anisotropic two-equation explicit algebraic Reynolds stress model (EARSM). A hybrid RANS–large eddy simulation (LES) model is also used. Computational results for global flow quantities are discussed and compared with experimental data. These quantities are in good agreement with the measured data. The hybrid RANS–LES model allows to capture the evolution of the tip vortices. For the INSEAN E779A model, the instability of the wake is only predicted with a hybrid RANS–LES model, and the position of these instabilities is in good agreement with the experimental visualizations.

1 Introduction

The prediction of the fluid dynamics interaction between propellers and the hull is very important for the improvement of ship performance since the interaction is directly related to vibrations, noise, and propulsion performances. In this context, the demand for the improvement of performance implies a rising interest in the development and application of detailed numerical tools.

The physical mechanisms that characterize the interaction between the propeller and the hull are very complex. However, even in the simpler case of an isolated propeller in a uniform flow, called open-water conditions, we are confronted with several numerical and physical challenges. In the propeller field, a number of viscous phenomena can be identified including blade and hub boundary layers, flow separation on the blade, hub and tip vortices, viscous wake, etc. Therefore, the study of these flow characteristics is essential for accurate prediction of the propulsion performance. In this paper, we only focus on the open-water

conditions. With a pushing propeller in straight-ahead flow, the flow is characterized by two vortex systems: one generated by the tip of the blade and the second emanated from the hub. A comprehensive description of the state of the art can be found in the study of Felli et al. [1], who experimentally investigated the flow around a propeller in water tunnel. These authors studied the mechanisms that trigger the instability of wake and investigated the dependence of the vortex pairing and grouping on the mutual vortex distance.

Based on a numerical point of view, the reliability of such numerical predictions can be questioned. It is difficult to control numerical diffusion when intense and localized three-dimensional structures are concerned. The flow in the core of the vortex is characterized by rotation, streamline curvature effects which are not adequately modeled by classical eddy-viscosity-based turbulence models. Unsteady hybrid large eddy simulation (LES) turbulence closures like detached eddy simulation (DES) appear attractive, see Muscari et al. [2].

Most studies only consider the case of a propeller in straight-ahead flow. However, under real conditions, a working propeller operates behind a ship usually in a complex wake, so that the propeller shows quite different hydrodynamic performance. Moreover, the consequence of the disturbance of the ship is that the

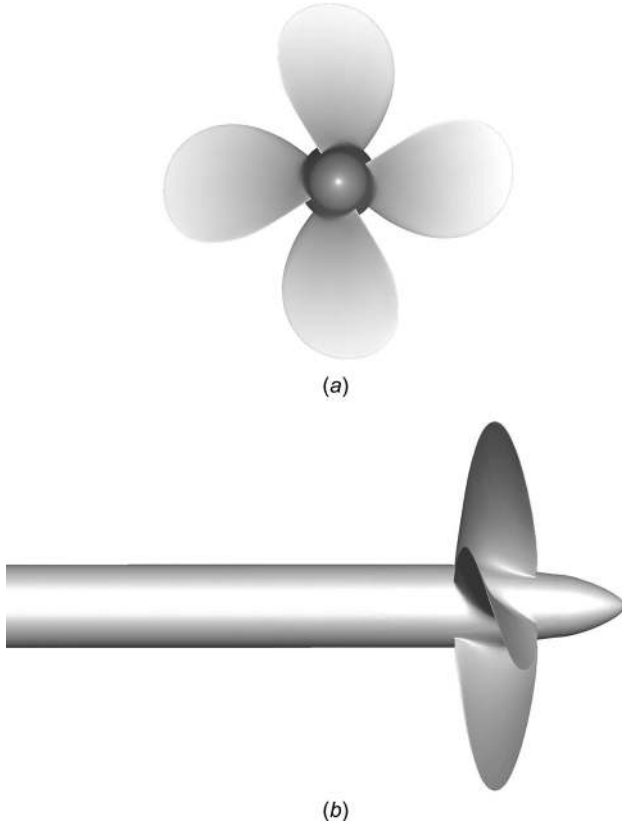


Fig. 1 INSEAN E779 model: (a) front view and (b) side view

Table 1 INSEAN E779 model: geometric parameters

Main particulars	Symbol	Value
Diameter	D	0.227 m
Number of blades	Z	4
Pitch ratio	P/D	1.1
Rake	i	$4^{\circ}35'$
Expand area ratio	EAR	0.689
Hub ratio	D_{H}/D	0.200

angle of attack is different from blade to blade, and the loads acting on the blades in axial direction are not symmetric.

Few authors have reported on hydrodynamic characteristics of a marine propeller in oblique flow. El Moctar and Bertram [3] used a Reynolds-averaged Navier–Stokes (RANS) solver to investigate the flow around a four-bladed modern propeller at oblique angles up to 12 deg. They found that the forces oscillate and the frequency of the oscillations increases with the angle of attack. Krasilnikov et al. [4] used an unsteady RANS method to investigate the blade forces acting on a podded propeller operating in oblique flow conditions. They found that blades of pulling propeller experience comparable amplitudes and load levels at positive and negative heading angles, being mainly affected by the cross-flow. The amplitudes and load levels on the blades of a pushing propeller are different at positive and negative headings due to the interaction of the propeller with the separated strut wake. Shamsi and Ghassemi [5] evaluated the performance of a podded propulsor in straight and azimuthing condition by using an RANS approach with moving reference frame. They found that the propeller thrust coefficient and the torque coefficient increase with increasing yaw angles. Their results also indicate that side force coefficients increase with increasing yaw angle and velocity advance ratio. Dubbioso et al. [6,7] analyzed the performance of the Istituto Nazionale per Studi ed Esperienze di Architettura Navale (INSEAN) E779A propeller model in oblique flow by

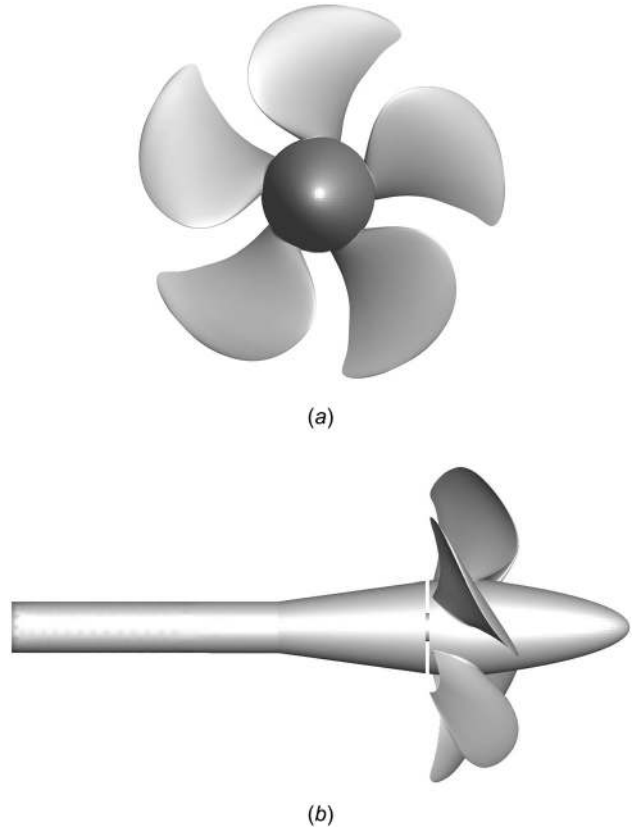


Fig. 2 PPTC model: (a) front view and (b) side view

Table 2 PPTC model: geometric parameters

Main particulars	Symbol	Value
Diameter	D	0.250 m
Number of blades	Z	5
Pitch ratio	P/D	1.635
Expand area ratio	EAR	0.150
Skewed angle	θ_{eff}	18.80 deg

unsteady RANS and dynamically overlapping grid approach. Their main focus is on hydrodynamic loads that act on a single blade. They also discuss the flow features around the propeller. Unfortunately, due to the lack of experiments in oblique flow conditions, they did not perform a validation of the numerical computations. Yao [8] investigated the hydrodynamic performance of a six-bladed propeller in oblique flow. The hydrodynamic forces and moment showed a good agreement with the experimental data under no cavitation condition or under weak cavitation condition.

The purpose of this paper is to conduct such a validation of the flow around an isolated propeller in straight-ahead flow and oblique flow to compare statistical turbulence closures and a hybrid LES methodology to draw conclusions about the requirements in terms of physics. The present paper is organized as follows. The test cases are presented followed by the numerical method. The computational fluid dynamics results are presented for comparison and validation, as well as flow field analysis. Finally, some concluding remarks are made.

2 Test Cases

In this paper, two propellers models are used: the INSEAN E779A model and the Potsdam Propeller Test Case (PPTC) model.

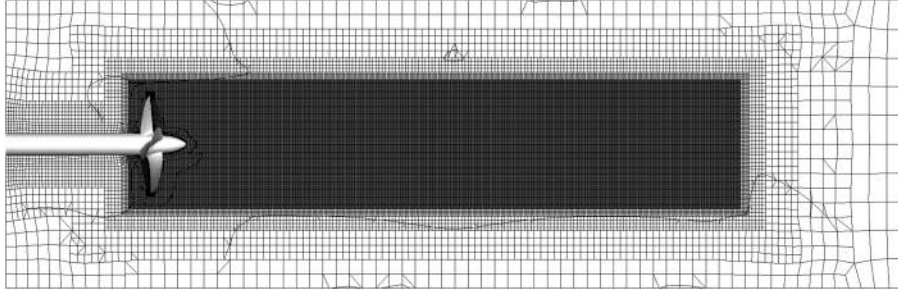


Fig. 3 INSEAN model: view of the mesh in the plane $Y = 0$

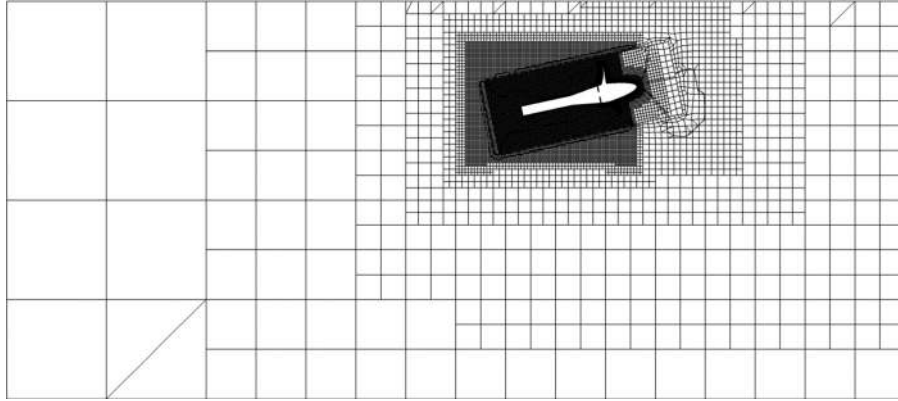


Fig. 4 PPTC model: view of the mesh in the plane $Y = 0$

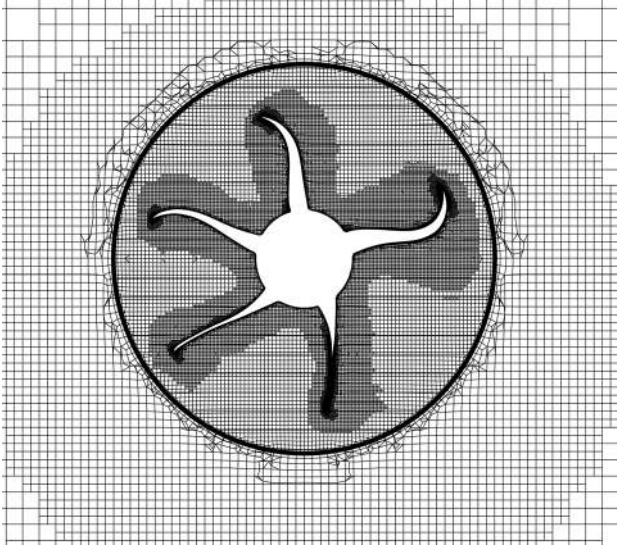


Fig. 5 PPTC model: view of the mesh in the plane $X = 0$

2.1 INSEAN E779A Model. The INSEAN E779A model is a four-bladed, fixed-pitch, right-handed propeller characterized by a nominally constant pitch distribution and a very low skew angle. The diameter of the propeller is $D = 0.227$ m. The propeller is presented in Fig. 1, and the main geometrical features are reported in Table 1.

In this paper, the rotational speed of the propeller is kept fixed to a value of $n = 25$ rps, and the different advance coefficients $J = U_\infty / (nD)$ are obtained by changing the inflow velocity U_∞ . The Reynolds number, $Re = 1.78 \times 10^6$, is based on the radius of the propeller ($R = D/2 = 0.1135$ m) and the velocity of the tips of the blades ($U_{ref} = n\pi D \equiv 17.829$ m/s).

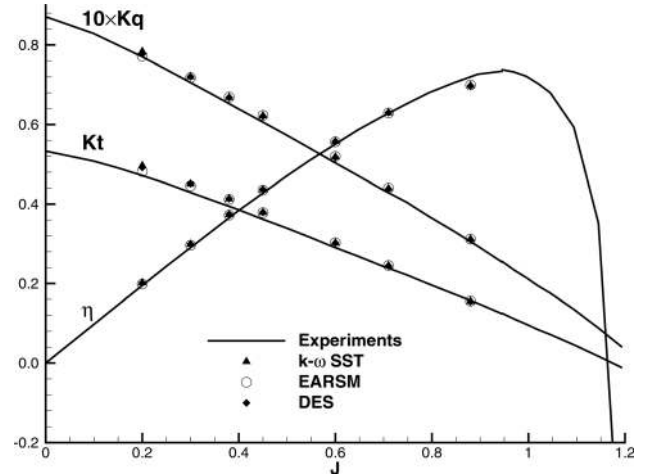


Fig. 6 INSEAN model: open-water characteristics

2.2 Potsdam Propeller Test Case Model. The PPTC model is a five-bladed right-handed propeller which is a controllable pitch propeller designed to generate a stable tip vortex. The diameter of the propeller is $D = 0.250$ m. The propeller is presented in Fig. 2, and the main geometrical features are reported in Table 2. The blade 1 is the blade at 12 o'clock position in the initial configuration which corresponds to the angle $\theta = 0$ deg.

In this study, the number of revolutions per second is constant and is $n = 15$ rps. The different advance coefficients, J , are obtained by changing the inflow velocity. The Reynolds number, $Re = 1.39 \times 10^6$, is based on the radius of the propeller ($R = 0.125$ m) and the velocity of the tips of the blades ($U_{ref} = n\pi D \equiv 11.781$ m/s). The propeller has an incidence inclination of 12 deg toward the inflow direction.

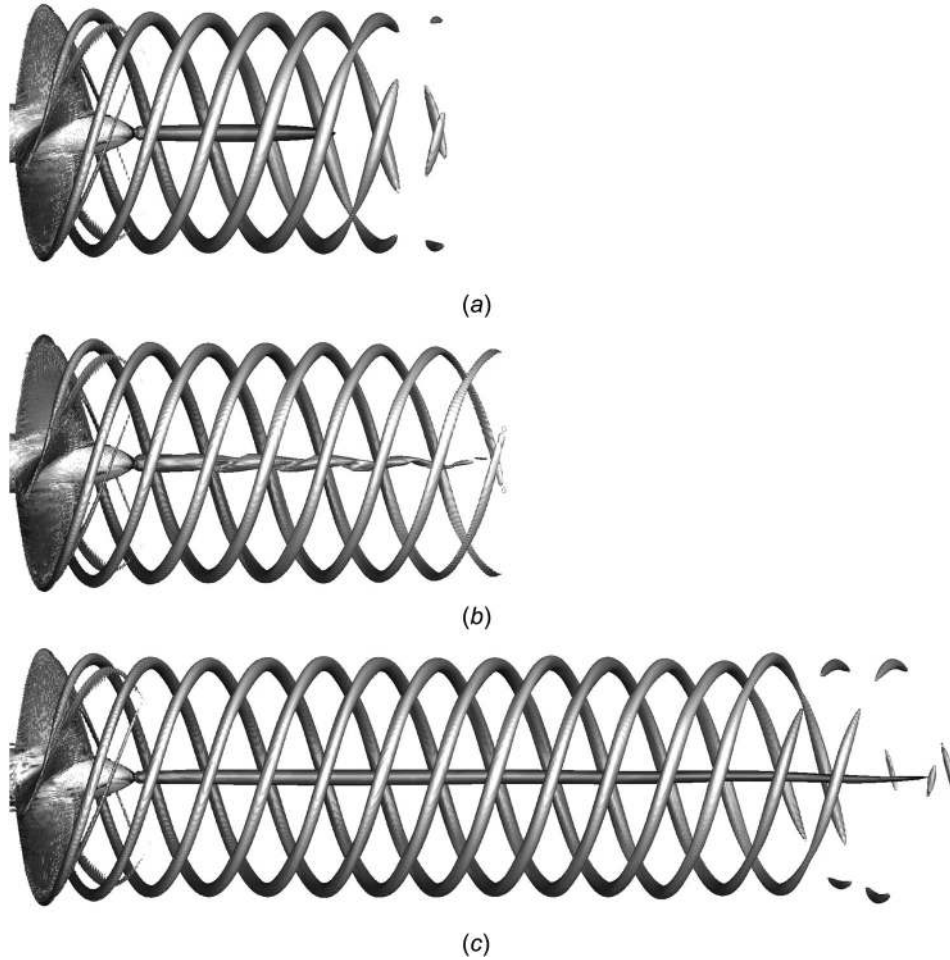


Fig. 7 INSEAN model: $J = 0.71$ —visualization of the vortical structures ($\lambda_2 = -2$): (a) $k-\omega$ shear stress transport (SST), (b) EARSM, and (c) DES

3 ISIS-CFD at Glance

The solver ISIS-CFD, available as a part of the FINETM/Marine computing suite, is an incompressible unsteady Reynolds-averaged Navier–Stokes method mainly devoted to marine hydrodynamics. The method features several sophisticated turbulence models: Apart from the classical two-equation $k-\epsilon$ and $k-\omega$ models, the anisotropic two-equation explicit algebraic Reynolds stress model (EARSM), as well as Reynolds stress transport models, is available [9]. All models are available with wall function or low Reynolds near wall formulation. Hybrid RANS–LES turbulence models based on DES are also implemented and have been validated on automotive flow characterized by large separation [10]. Additionally, several cavitation models are available in the solver.

The solver is based on finite volume method to build the spatial discretization of the transport equations. The unstructured

discretization is face-based. While all unknown state variables are cell-centered, the system of equations used in the implicit time-stepping procedure are constructed face by face, and the contribution of each face is then added to the two cells next to the face. This technique poses no specific requirements on the topology of the cells. Therefore, the grids can be completely unstructured: Cells with an arbitrary number of arbitrarily shaped faces are accepted. Pressure–velocity coupling is enforced through a Rhie and Chow semi-implicit method for pressure linked equations-type method: At each time step, the velocity updates come from the momentum equations, and the pressure is given by the mass conservation law, transformed into a pressure equation. In the case of turbulent flows, transport equations for the variables in the turbulence model are added to the discretization.

Free-surface flow is simulated with a multiphase flow approach: The water surface is captured with a conservation equation for the

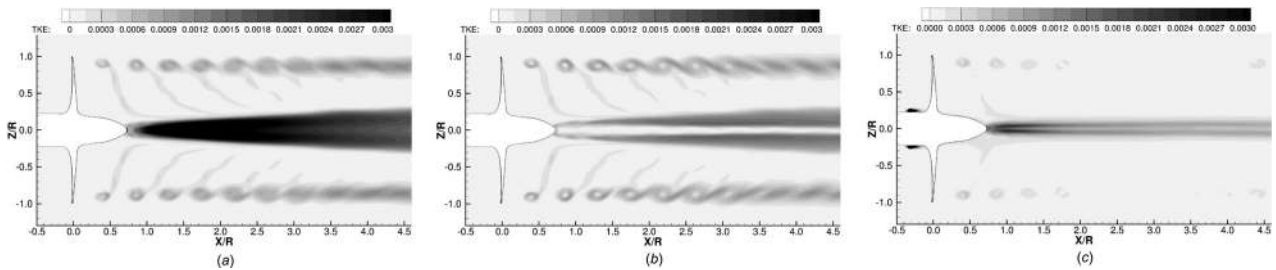


Fig. 8 INSEAN model: $J = 0.71$ —TKE in the plane $Y = 0$: (a) $k-\omega$ SST, (b) EARSM, and (c) DES

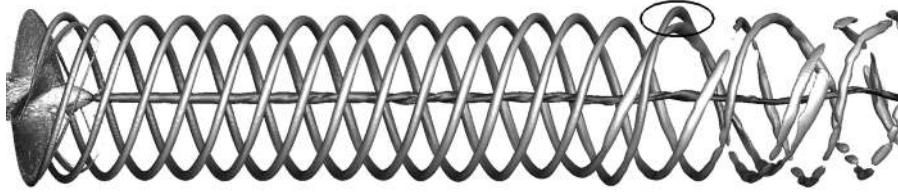


Fig. 9 INSEAN model: $J = 0.71$ —instantaneous visualization of the vortical structures with DES approach ($\lambda_2 = -2$)

volume fraction of water, discretized with specific compressive discretization schemes [11]. The technique included for the six degrees-of-freedom simulation of ship motion is described by Leroyer and Visonneau [12]. Time integration of Newton's law for the ship motion is combined with analytical weighted analogy grid deformation and rigid motion to adapt the fluid mesh to the moving ship. To enable relative motions of appendages, propellers or bodies without having recourse to overlapping grids, a sliding grid approach has been implemented. Propellers can be modeled

by actuator disk theory, by coupling with boundary element codes (RANS–boundary element method coupling [13]) or with direct discretization through, e.g., the rotating frame method or sliding interface approaches.

Finally, an anisotropic automatic grid refinement procedure has been developed, which is controlled by various flow related criteria [14]. Parallelization is based on domain decomposition. The grid is divided into different partitions, which contain the cells. The interface faces on the boundaries between the partitions are

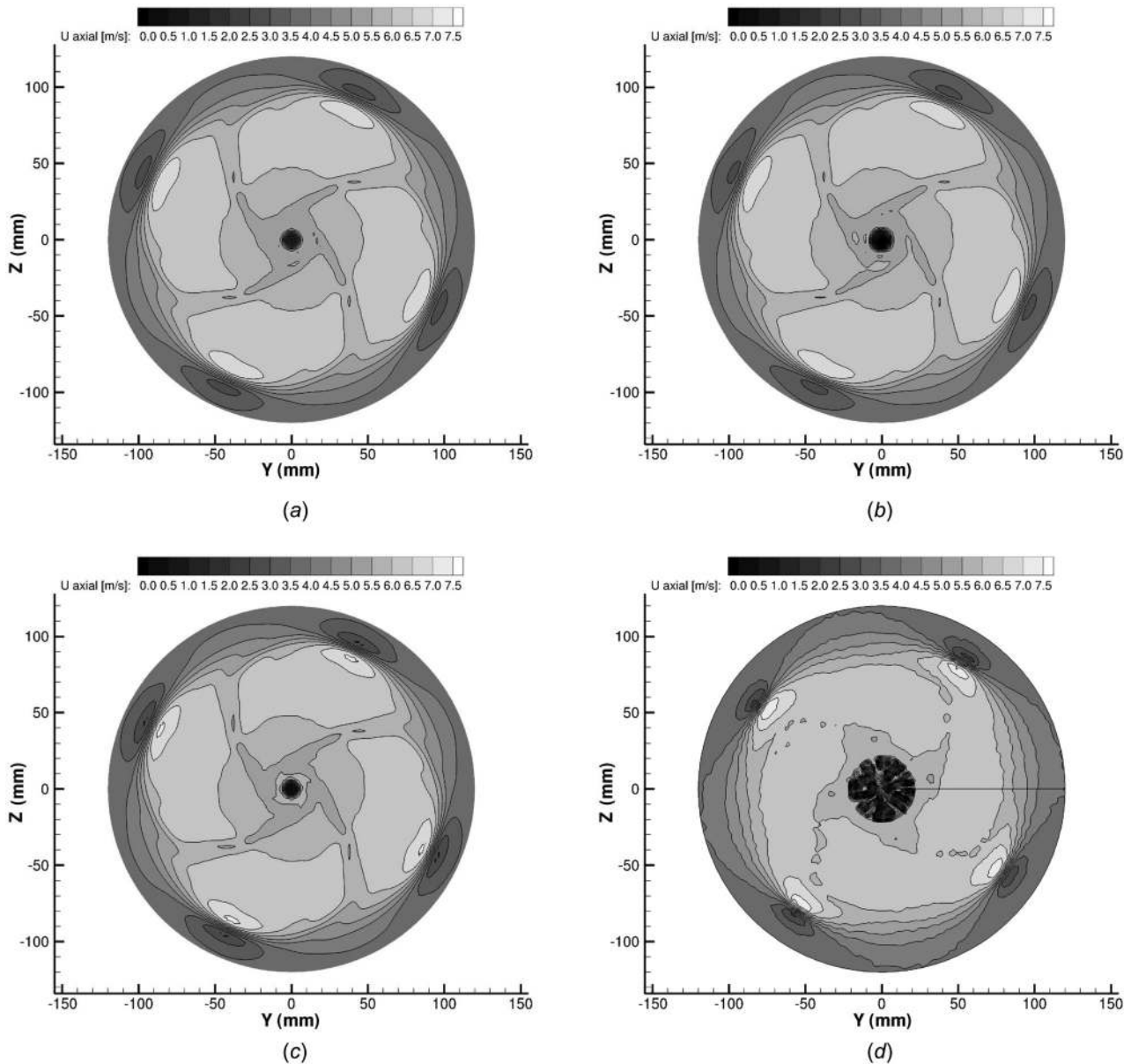


Fig. 10 INSEAN model: $J = 0.71$ —axial velocity at $X = 110$ mm in the wake of the propeller: (a) $k-\omega$ SST, (b) EARSM, (c) DES, and (d) experiments

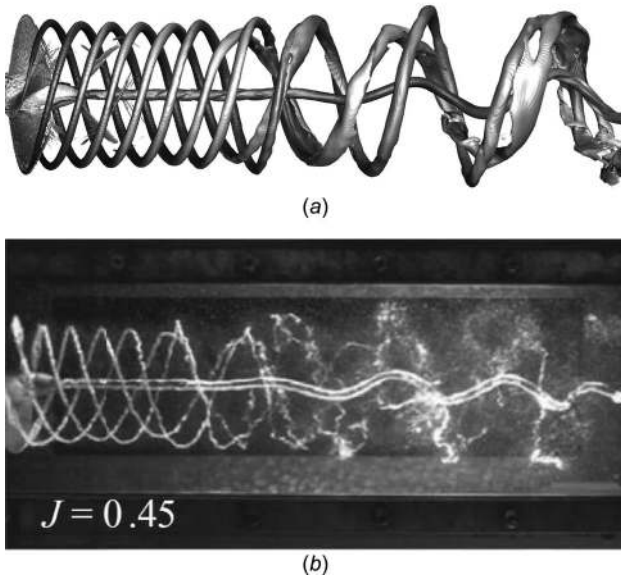


Fig. 11 INSEAN model: $J = 0.45$ —comparison of vortical structures between a DES approach and experiments ($\lambda_2 = -2$): (a) DES (instantaneous view) and (b) experimental view (Fig. 8 in Ref. [1])

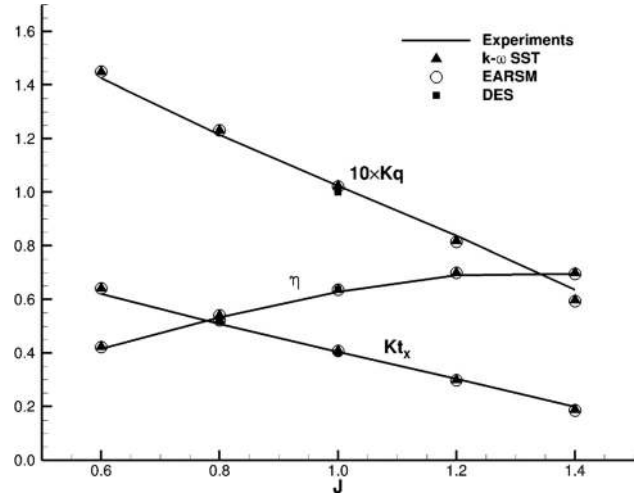


Fig. 13 PPTC model: open-water characteristics

shared between the partitions; information on these faces is exchanged with Message Passing Interface protocol. The method works with the sliding grid approach, and the different subdomains can be distributed arbitrarily over the processors without any loss of generality. Moreover, the automatic grid refinement procedure is fully parallelized with a dynamic load balancing working transparently with or without sliding grids.

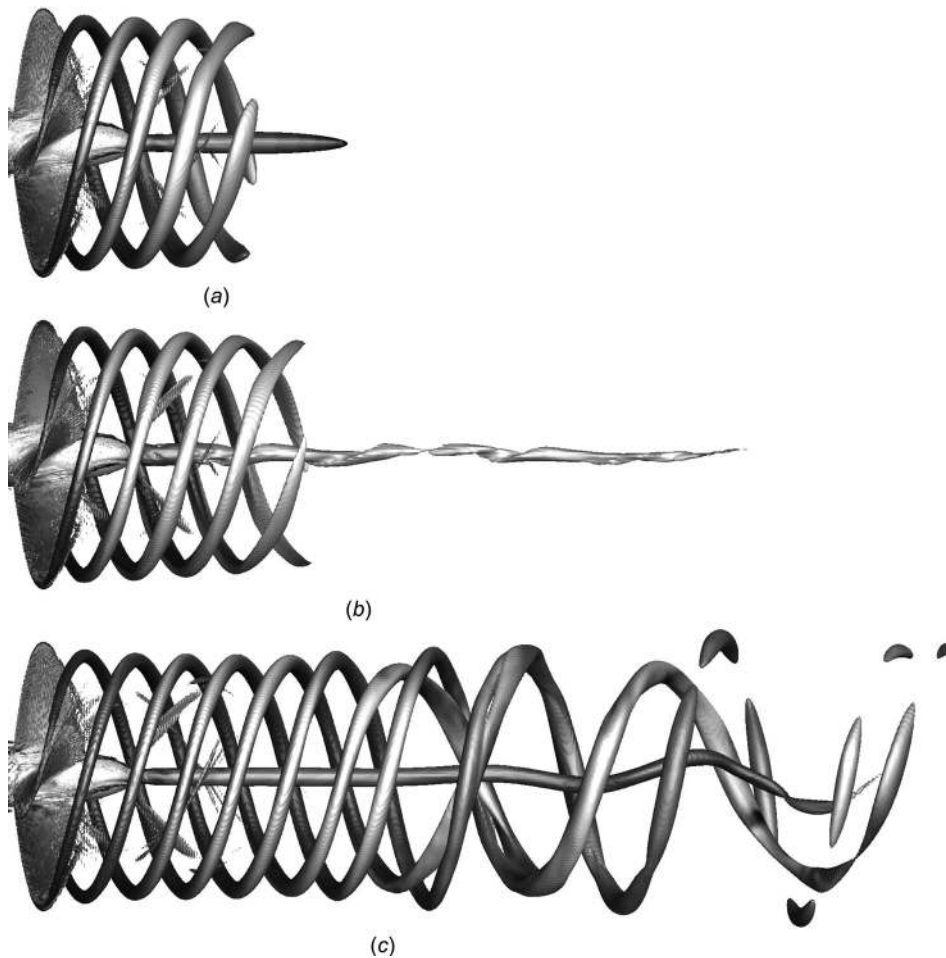


Fig. 12 INSEAN model: $J = 0.45$ —visualization of the vortical structures ($\lambda_2 = -2$): (a) $k-\omega$ SST, (b) EARSM, and (c) DES

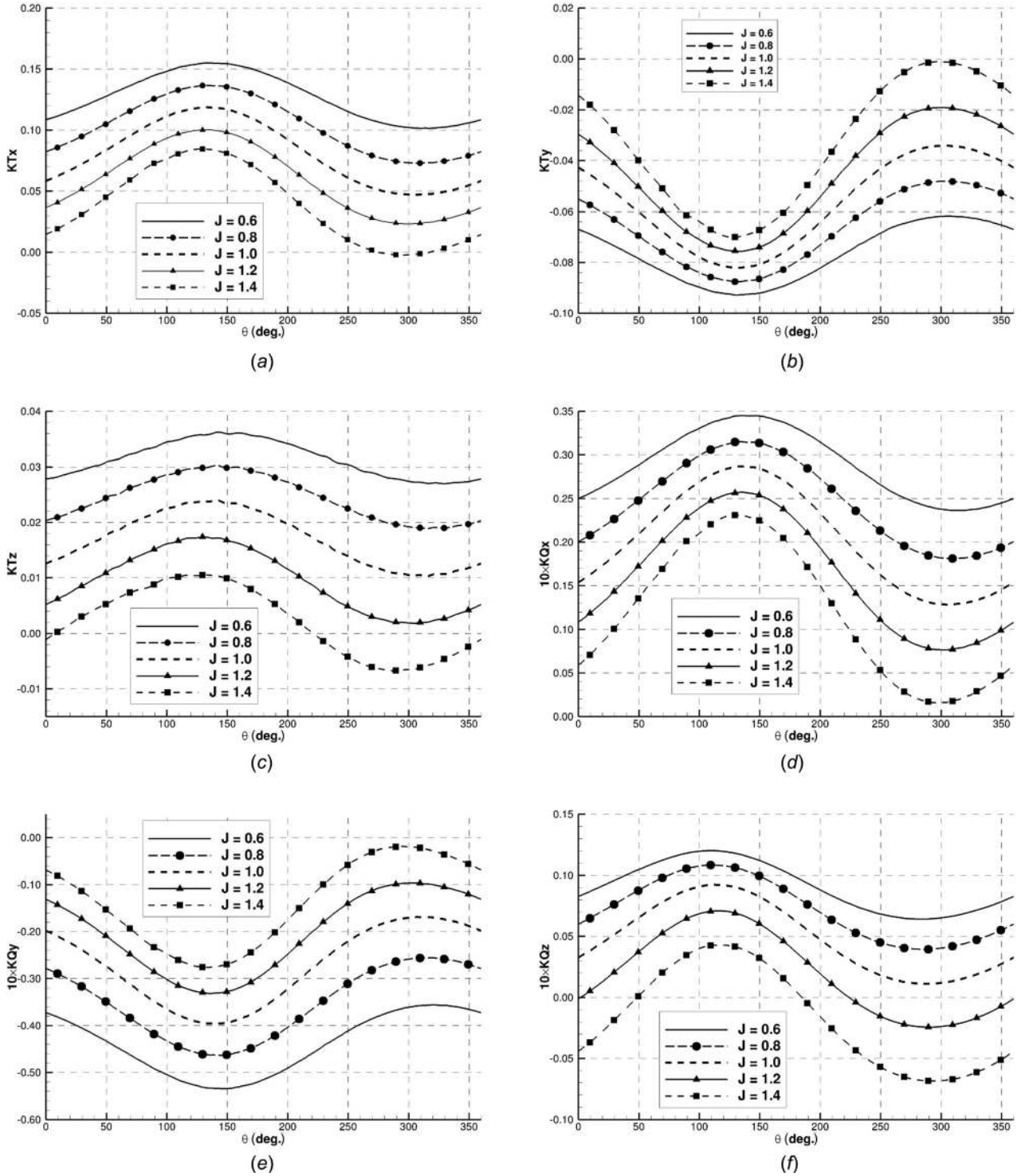


Fig. 14 PPTC model: force and moment coefficients on a single blade: (a) KTx , (b) KTy , (c) KTz , (d) KQx , (e) KQy , and (f) KQz

4 Numerical Simulation Setup

For both cases, the computational mesh is created with HexpressTM, an automatic unstructured mesh generator. This software generates meshes containing only hexahedrons.

4.1 INSEAN E779A Model. For this model, a pusher configuration is investigated that means the hubcap is in the wake of the propeller. The computational domain consists of a cylindrical domain, whose diameter is three times the propeller diameter, and

the length is 9.18 times the propeller diameter. It starts $3.96R$ before the propeller plane.

The mesh consists of 21.42×10^6 cells. The number of faces for each blade is approximately 38,100. The average wall normal resolution on the blades is $y^+ = 0.6$ with a maximum around the tip, in the order of 1.8. A box including the propeller and extending up to six diameters in the wake is added to capture the vortices. In this box, the cells are isotropic and the size is $0.0105R$, see Fig. 3.

For the RANS turbulence models ($k-\omega$ SST or EARSM), the solution is a steady solution while for DES computations, this

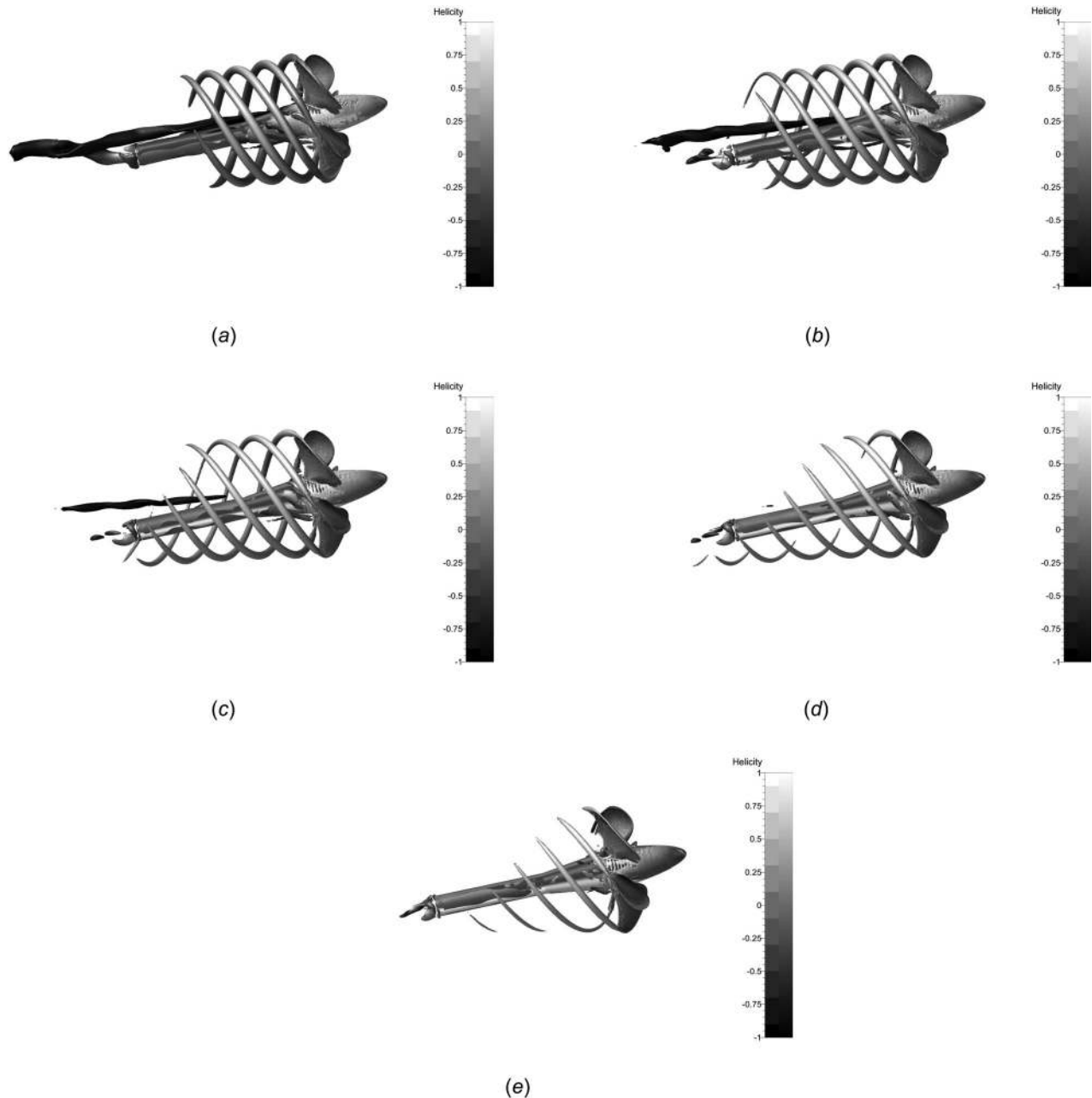


Fig. 15 PPTC model: visualization of the vortical structures ($\lambda_2 = -2$) at $\theta = 50.7$ deg with the $k-\omega$ SST turbulence model: (a) $J = 0.60$, (b) $J = 0.80$, (c) $J = 1.00$, (d) $J = 1.20$, and (e) $J = 1.40$

approach is unsteady and the time step is $\Delta t = 3 \times 10^{-5}$ s, which corresponds to a rotation of 0.27 deg. The time-averaged flow is obtained in approximately nine rotations for DES computations.

4.2 Potsdam Propeller Test Case Model. For this model, the propeller is operating in a pull configuration with the hubcap pointing upstream. As the propeller is in incidence, in order to take into account the rotation of the propeller, the computational domain is decomposed into two regions: the rotating region close to the propeller and the stationary region. The total length of the computational domain is $15D$ with the inlet located $5D$ in front of the propeller rotation center. The computational domain has a width of $10D$ and a height of $6.5D$ with the top located $1.5D$ above the propeller rotation center.

The mesh consists of 28.74×10^6 cells with 28.25×10^6 cells in the rotating region. The number of faces for each blade is approximately 220,100. The average wall normal resolution on the blades

is $y^+ = 0.3$ with a maximum around the tip, in the order of 2.0. In the rotating mesh, the cells are isotropic and the size is $0.025R$, see Fig. 4. Figure 5 shows a partial view of the mesh in a plane $X = 0$, which is the center of the propeller. The thick circle in the figure represents sliding interfaces.

As the propeller is in incidence, an unsteady approach is used, and the time step, for the RANS turbulence models, is $\Delta t = 1.889 \times 10^{-3}$ s, which corresponds to a rotation of 1 deg while, for the hybrid RANS-LES model, the time step is $\Delta t = 4.6296 \times 10^{-5}$, which corresponds to a rotation of 0.25 deg.

5 Results and Discussion

5.1 INSEAN E779A Model. In order to compare different turbulence models for the prediction of the flow around the propeller, the open-water characteristics of the model are investigated. Several numerical results for different values of the

advance coefficient J are compared with the experimental data [1], see Fig. 6. Concerning the thrust coefficient $Kt = T/(\rho n^2 D^4)$, where T is the thrust of the propeller and ρ is the density of the water, the torque coefficient $Kq = Q/(\rho n^2 D^5)$, where Q is the torque, and the propeller open-water efficiency $\eta = Kt/Kq \times J/(2\pi)$; the predictions obtained with the different turbulence models are very similar and differ by less than 5% for the low values of the advance coefficient and by less than 3% for the high value of J . These numerical simulations are also in good agreement with the experimental data.

One of the objectives is to evaluate the ability of the turbulence model to reproduce some of the findings of Felli et al. [1]. The analysis of the flow field is carried out for two values of the advance coefficient, $J = 0.71$ and 0.45 .

A general view of the wake of the propeller, for the advance coefficient $J = 0.71$, is given in Fig. 7, which presents an isosurface of the dimensionless value $\lambda_2 = -2$ of the second largest invariant of $S^2 + \Omega^2$ (S and Ω being the symmetric and antisymmetric component of $\nabla \mathbf{u}$) colored by the helicity. The acceleration of the flow behind the propeller causes a slight reduction of the radial position of the vortex cores. Then, the helices formed by the tip vortices remain located on a circular cylinder. RANS models yield tip vortices but they vanish more or less rapidly in the wake depending on the turbulence model used. With the DES approach, the tip vortices are maintained much further in the wake. These remarks are also observed by Muscari et al. [2].

Figure 8 presents the turbulent kinetic energy (TKE) in the plane $Y = 0$. For the DES approach, this quantity presents the average value of the modeled part and of the resolved part. The RANS simulations predict a small value of TKE near the tip of the blade which grows rapidly in the vortex core. The values around the vortex core increase along the filament. On the contrary, the DES approach produces a high TKE near the tip but the level vanishes quickly in the wake, and the level is lower than those observed with an RANS approach. When the turbulence model becomes more anisotropic, the vortex core becomes laminar. This remark has been also noted by Wells et al. [15] who used Spalart–Allmaras model and full Reynolds stress model to simulate tip vortices. They observed that the predicted Reynolds stresses show a laminar vortex core.

The detailed frequency analysis performed in the experimental work illustrates the process of energy transfer from the blade harmonic to the shaft at nearly at $X = 7R$ [1], owing to vortex grouping. In the numerical simulation with the DES approach, the vortex grouping, marked by a thick ellipse, appears nearly $7.2R$, as shown in Fig. 9. The instability of the propeller wake is characterized by a gradual deformation of the hub vortex and a sudden destabilization of the helical path of the tip vortices. The hub vortex describes a spiral geometry of progressively increased amplitude, and the tip vortices tend to group where the hub vortex spiral is the local maximum.

Figure 10 illustrates a comparison of the velocity distribution in the wake of the propeller at $X = 110$ mm. The velocity is underestimated with the RANS simulations, see Figs. 10(a) and 10(b), $k-\omega$ SST and EARSM, respectively, while the results obtained

with the DES, see Fig. 10(c), are in better agreement with the experimental data [16], see Fig. 10(d). The maximum of velocity corresponds to the position of the tip vortices. These areas are located at the same position for the numerical results while for the experimental data, they are turned off few degrees.

These differences between the positions of the maximum of velocity are due to the spiral-to-spiral distance which is not similar, as is shown in Fig. 11, which presents an instantaneous view of the vortical structure obtained with a DES approach and the visualization of Felli et al. [1] for another advance coefficient $J = 0.45$. These figures are very similar and present the pairing of the vortices. The difference between the numerical results and the experimental visualization is the spiral-to-spiral distance. In the numerical simulation, this distance is shorter than that observed in experiments. However, the numerical spiral-to-spiral distance is in agreement with the numerical simulation of Muscari et al. [2], which used another flow solver with another mesh.

To compare all turbulence models for this advance coefficient, the averaged flow for the DES approach is presented with the RANS results in Fig. 12. For the RANS results, the characteristics of the flow are the faster deformation of the wake and the stronger tip vortices. Even if the tip vortices are stronger than those predicted with $J = 0.71$, they are resolved over a short distance. This trend is also confirmed by another numerical result [2]. The DES method permits to predict more extended vortices and shows both the onset of the vortex instability and the start of the pairing process.

5.2 Potsdam Propeller Test Case Model. This propeller model has an inclination of 12 deg with the upstream velocity. Thus, the propeller performances are evaluated in the propeller coordinate system, that is to say, in the hub frame reference.

The open-water characteristics, obtained with the two RANS turbulence models and the hybrid RANS–LES model, are compared with the experimental data [17] in Fig. 13. The agreement is the same order than the previous propeller model. The prediction of the thrust differs and is overestimated by 3.2% for the lowest value of J and underestimated by 5.2% for the higher value of J while the torque coefficient is overestimated by 1.6% for the lowest value of J and underestimated by 6% for the highest value of J .

As the propeller is in incidence, the loads generated by the blade are not constant during the revolution. This behavior is highlighted in Fig. 14, representing the forces and moments on the blade 1 in propeller coordinate system. The mean value of these coefficients decreases as the coefficient J increases while the amplitude of these coefficients increases. It can be observed that the thrust, KT_x , and the vertical force, KT_z , developed during the blade passage on the first half of the disk, $0 \text{ deg} < \theta < 180 \text{ deg}$, are smaller, in absolute value, than those developed in the second half of the disk, $180 \text{ deg} < \theta < 360 \text{ deg}$. The lateral force, KT_y , is phase-shifted with respect to the other ones by a quarter of a cycle, i.e., $\pi/2$. Similar comments hold for the moments.

A general view of the wake of the propeller, according to the advance coefficient J , is given in Fig. 15, which presents an

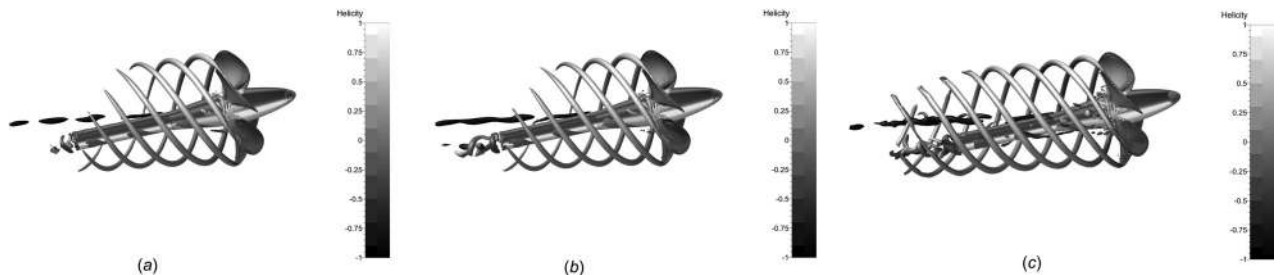


Fig. 16 PPTC model: $J = 1.00$ —visualization of the vortical structures ($\lambda_2 = -2$) at $\theta = 14.74$ deg: (a) $k-\omega$ SST, (b) EARSM, and (c) DES

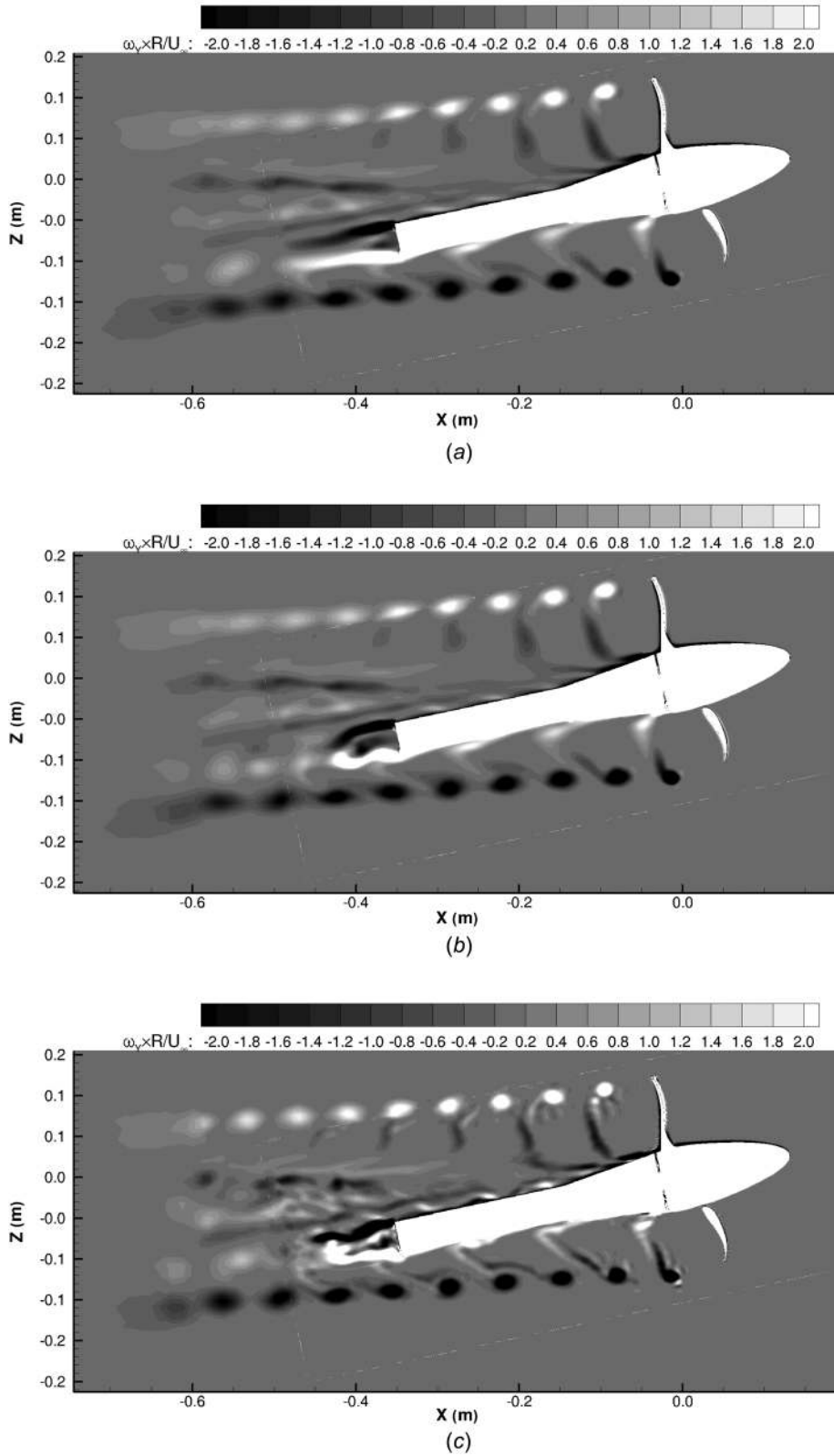


Fig. 17 PPTC model: $J = 1.00$ —vorticity in the plane $Y = 0$ at $\theta = 14.74$ deg: (a) $k-\omega$ SST, (b) EARSM, and (c) DES

isosurface of the dimensionless value $\lambda_2 = -2$ colored by the helicity obtained with the $k-\omega$ SST turbulence model. For all views, the blade 1 has the same position, and the angle is 50.7 deg. Some features of the tip vortices are similar to the previous propeller model. As the advance coefficient increases, the size of the tip

vortices is weaker, and these vortices are more and more dissipated in the wake of the propeller. A difference with the previous propeller in straight-ahead flow is the prediction of a vortex generated at the root of the blade but this vortex disappears when the advance coefficient increases.

Figure 16 shows the influence of the turbulence modelization for the advance coefficient $J=1.0$ at the angle $\theta=14.7$ deg. As for the previous propeller, with the hybrid RANS–LES model, the tip vortices are maintained much further in the wake. For this numerical simulation, the tip vortices obtained with the DES is well predicted in the rotating region. Then, these vortices vanish because the mesh in the stationary region is not enough fine. The separation, generated at the root of the blade, in the beginning of the motion disappears at the beginning of the second part of the motion.

The lateral vorticity, Y -component, for the advance coefficient $J=1.0$, is presented, in the plane $Y=0$, in Fig. 17 according to the turbulence model used. The extreme values are more pronounced with the hybrid RANS–LES model than those obtained with the RANS model. This observation has been already done by Guilmineau et al. [18] for the numerical simulation of the flow around the INSEAN propeller with the same turbulence models. The lower tip vortex envelope is practically unaffected by the incidence of the propeller. For the upper tip vortex envelope, the alignment with the upstream flow occurs later in the wake of the propeller.

6 Conclusions

The capabilities of numerical simulations with various turbulence closures, RANS and DES, using ISIS-CFD flow solver, to predict the complex flow past an isolated propeller have been presented in this paper. Two propellers have been investigated: the INSEAN E779A model and the PPTC model. The first model is in straight-ahead flow conditions while the second in oblique flow conditions.

For both propeller models, the numerical simulations, regardless of the turbulence model used, predict similar results for the global quantities, such as the thrust and the torque, and they are in good agreement with the measured data. However, the prediction of the wake is not exactly the same; it depends on the turbulence model used. The hybrid RANS–LES approach allows to capture the evolution of the tip vortices if the mesh is fine enough. For the INSEAN E779A model, the DES model is able to predict the initial stages of the instability pattern with two consecutive filaments grouping their relative position, which agree reasonably well with the flow visualizations.

Acknowledgment

This work was granted access to the HPC resources of CINES/IDRIS under the allocations 2014-2a0129 and 2015-2a0129 made by GENCI.

References

- [1] Felli, M., Camusi, R., and Felice, F. D., 2011, "Mechanisms of Evolution of the Propeller Wake in the Transition and Far Fields," *J. Fluid Mech.*, **682**, pp. 5–53.
- [2] Muscari, R., Mascio, A. D., and Verzicco, R., 2013, "Modeling of Vortex Dynamics in the Wake of a Marine Propeller," *Comput. Fluids*, **73**, pp. 63–79.
- [3] El Moctar, O. M., and Bertram, V., 2000, "RANS Simulation of Propeller in Oblique Flow," Third Numerical Towing Tank Symposium (NUTTS), Tjarno, Sweden, Sept. 9–13, pp. 46–48.
- [4] Krasilnikov, V., Zhang, Z., and Hong, F., 2009, "Analysis of Unsteady Propeller Blade Forces by RANS," First International Symposium on Marine Propulsors (SMP), Trondheim, Norway, June 9, pp. 251–261.
- [5] Shamsi, R., and Ghassemi, H., 2013, "Numerical Investigation of Yaw Angle Effects on Propulsive Characteristics of Podded Propulsors," *Int. J. Nav. Archit. Ocean Eng.*, **5**(2), pp. 287–301.
- [6] Dubbioso, G., Muscari, R., and Mascio, A. D., 2013, "Analysis of the Performance of a Marine Propeller Operating in Oblique Flow," *Comput. Fluids*, **75**, pp. 86–102.
- [7] Dubbioso, G., Muscari, R., and Mascio, A. D., 2014, "Analysis of the Performance of a Marine Propeller Operating in Oblique Flow. Part 2: Very High Incidence Angles," *Comput. Fluids*, **92**, pp. 56–81.
- [8] Yao, J., 2015, "Investigation on Hydrodynamic Performance of a Marine Propeller in Oblique Flow by RANS Computation," *Int. J. Nav. Archit. Ocean Eng.*, **7**(1), pp. 56–69.
- [9] Deng, G. B., and Visonneau, M., 1999, "Comparison of Explicit Algebraic Stress Models and Second-Order Turbulence Closures for Steady Flow Around Ships," Seventh Symposium on Numerical Ship Hydrodynamics, Nantes, France, July 19–22, pp. 4.4.1–4.4.15.
- [10] Guilmineau, E., Deng, G. B., and Wackers, J., 2011, "Numerical Simulation With a DES Approach for Automotive Flows," *J. Fluids Struct.*, **27**(5–6), pp. 807–816.
- [11] Queutey, P., and Visonneau, M., 2007, "An Interface Capturing Method for Free-Surface Hydrodynamic Flows," *Comput. Fluids*, **36**(9), pp. 1481–1510.
- [12] Leroyer, A., and Visonneau, M., 2005, "Numerical Methods for RANSE Simulations of a Self-Propelled Fish-Like Body," *J. Fluids Struct.*, **20**(7), pp. 975–991.
- [13] Deng, G. B., Queutey, P., Visonneau, M., and Salvatore, F., 2013, "Ship Propulsion Prediction With a Coupled RANS-BEM Approach," V International Conference on Computational Methods in Marine Engineering, Hamburg, Germany, May 29–31, pp. 541–551.
- [14] Wackers, J., Deng, G. B., Guilmineau, E., Leroyer, A., Queutey, P., and Visonneau, M., 2014, "Combined Refinement Criteria for Anisotropic Grid Refinement in Free-Surface Flow Simulation," *Comput. Fluids*, **92**, pp. 209–222.
- [15] Wells, J., Salem-Said, A., and Ragab, S. A., 2010, "Effects of Turbulence Modeling on RANS Simulations of Tip Vortices," AIAA Paper No. 2010-1104.
- [16] Felli, M., Guj, G., and Camusi, R., 2008, "Effect of the Number of Blades on Propeller Wake Evolution," *Exp. Fluids*, **44**(3), pp. 409–418.
- [17] Aktas, B., Turkmen, S., and Sampson, R., 2015, "Underwater Radiated Noise Investigations of Cavitating Propellers Using Medium Size Cavitation Tunnel Tests and Full-Scale Trials," Fourth International Symposium on Marine Propulsors (SMP'15), Austin, TX, May 31–June 4.
- [18] Guilmineau, E., Deng, G. B., Leroyer, A., Queutey, P., Visonneau, M., and Wackers, J., 2015, "Influence of the Turbulence Closures for the Wake Prediction of a Marine Propeller," Fourth International Symposium on Marine Propulsors (SMP), Austin, TX, May 31–June 4, pp. 177–183.